SCIENCE CHINA Materials ARTICLES

mater.scichina.com link.springer.com

Published online 13 October 2017 | doi: 10.1007/s40843-017-9118-3
Sci China Mater 2017, 60(12): 1253–1263

Influence of monovalent Bi^+ doping on real composition, point defects, and photoluminescence in $TlCdCl_3$ and $TlCdI_3$ single crystals

Daria N. Vtyurina[1], Polina A. Eistrikh-Geller[2], Galina M. Kuz'micheva[2], Victor B. Rybakov[3], Evgeny V. Khramov[4], Irina A. Kaurova[2*], Dmitry Yu. Chernyshov[5] and Vladimir N. Korchak[1]

ABSTRACT **The structural features and real compositions with point defects of Bi^+-doped $TlCdCl_3$ and $TlCdI_3$ single crystals, grown by the Bridgman-Stockbarger technique, are first studied using the X-ray diffraction, X-ray synchrotron radiation, and EXAFS/XANES spectroscopy. In the structures of Bi^+-doped $TlCdCl_3$ and $TlCdI_3$ crystals, the Cd, Cl, and I sites are found to be defect-free. The vacancies in the Tl sites and interstitial Bi atoms located in the vicinity of the Tl sites are detected in the structures of both samples. In the Bi^+-doped $TlCdCl_3$, the presence of a small amount of Bi^+ ions in the Tl^+ sites is possible. The correlation between photoluminescence bands and point defects in the refined structures are determined. Photoluminescence spectra and decay kinetics of the Bi^+-doped $TlCdCl_3$ and $TlCdI_3$ demonstrate that they are attractive materials for potential applications in photonics.**

Keywords: single crystal, growth, doping, crystal structure, point defects, photoluminescence

INTRODUCTION

Compounds doped with the Bi^+ ions can exhibit an effective photoluminescence (PL) in the near infrared spectral range (900 –1600 nm) and, hence, may be used in optical devices, in particular, new tunable lasers and optical amplifiers. These devices can find a wide application prospect in medicine (laser surgery) and metrology. A controlled synthesis of new optically active media requires an understanding of the formation mechanism of photoluminescent Bi^+ centers.

Subvalent bismuth compounds and cluster forms attract a great scientific interest [1–7]. Within the $6s^26p^2$ electron configuration, the Bi^+ cation possesses the $^3P_0$ ground electronic state and the $^3P_1$ and $^3P_2$ low lying excited states, the energy gap between these levels being due to a strong spin-orbit coupling [8]. An additional splitting of degenerate $^3P_1$ and $^3P_2$ states by the crystal field forms the energy diagram of Bi^+ impurity in the crystals, which determines its optical properties. The optical transition from the $^3P_1$ excited state to the ground state results in a long-lived (hundreds of microseconds) photoluminescence in the near infrared spectral region [9].

It is known that the low-valence (subvalent) Bi^+ cation can be obtained in acidic melts and solutions by the reduction reactions of trivalent bismuth compounds or *via* their synproportionation with metallic bismuth [10,11]. The location of Bi^+ ions in the crystal structures of the compounds has not been established. The presence of bismuth in the form of isomorphous impurity in the position of cations having the formal charge 1+ (K, Rb, Cs, Tl) was only assumed based on the close ionic radii of Bi^+ and these cations [12]. It is isomorphism and synthesis conditions that formed the basis for correlating the spectral bands with Bi^+ ions [13–18]. However, neither confirmation of isomorphous substitution of the above-mentioned components, nor consideration of any other possible Bi^+ locations in the crystal structures of Bi^+-containing compounds with different compositions can be found in the literature.

[1] Semenov Institute of Chemical Physics, Russian Academy of Sciences, Moscow 119991, Russia
[2] Institute of Fine Chemical Technologies, Moscow Technological University, Moscow 119571, Russia
[3] Lomonosov State University, Moscow 119992, Russia
[4] National Research Center «Kurchatov Institute», Moscow 123182, Russia
[5] Swiss-Norwegian Beamlines at the European Synchrotron Radiation Facility, Grenoble 38000, France
[*] Corresponding author (email: kaurchik@yandex.ru)

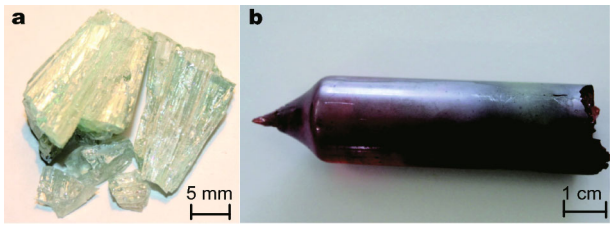

Figure 1 Photos of fragment of $TlCdCl_3$:Bi crystal (a) and $TlCdI_3$:Bi single crystal (b).

The purpose of our study was to determine the precise real compositions of $TlCdCl_3$ and $TlCdI_3$ single crystals doped with the Bi^+ ions and find their correlations with optical parameters.

EXPERIMENTAL SECTION

The Bi^+-doped $TlCdCl_3$ ($TlCdCl_3$:Bi) and $TlCdI_3$ ($TlCdI_3$:Bi) single crystals were grown by the Bridgman-Stockbarger technique (Fig. 1).

The initial batch for growth of $TlCdCl_3$:Bi crystal was composed of the TlCl, $CdCl_2$, and $BiCl_3$ with a molar ratio of 44.8:54.8:0.4. The initial components were placed into a quartz glass ampoule with the inner diameter of 20 mm together with a small amount of metallic bismuth taken in proportion of $BiCl_3$/Bi = 1, which has been determined experimentally to form the univalent bismuth [19]. All the procedures of weighing of the reagents and placing them into the ampoule were carried out under dry inert gas atmosphere. Then, the ampoule was evacuated and sealed off at the preformed waist. The single-crystal grew at an ampoule lowering speed of 1 mm h^{-1}. During crystal growth, the temperature in the upper zone of the furnace was maintained at 460°C. The as-grown $TlCdCl_3$:Bi single crystal with a diameter of 20 mm and a length of 100 mm was pale blue. According to the energy-dispersive X-ray microanalysis (FEI Quanta 200), the Tl, Cd, and Cl content is 20.11, 17.63, 58.74 at.%, respectively. According to inductively coupled plasma mass spectrometry data (Thermo Scientific iCAP Q ICP-MS), the content of bismuth impurity in the resulting sample is 0.1 at.%.

The above-described technique was used for the $TlCdI_3$:Bi single crystal growth. The initial batch for growth of $TlCdI_3$:Bi crystal was composed from TlI, CdI_2, and BiI_3 with a molar ratio of 49.9:49.9:0.2, respectively. The metal Bi in proportion BiI_3/Bi = 1 was also introduced. During crystal growth, the temperature in the upper zone of the furnace was maintained at 263°C. The as-grown $TlCdI_3$:Bi single crystal with a diameter of 20 mm and a length of 100 mm was dark red (Fig. 1b).

The X-ray diffraction (XRD) analysis of $TlCdX_3$:Bi (X = Cl, I) microcrystals ~0.1×0.1×0.1 mm^3 in size was performed with an Enraf-Nonius CAD-4 single-crystal diffractometer at room temperature (Ag K_α, graphite monochromator, ω-scan mode). To reduce the error associated with the absorption, the XRD data were collected over the entire Ewald sphere. The preliminary XRD data processing was carried out using the WinGX pack [20]. The atomic coordinates, anisotropic displacements parameters of all atoms, and occupancies of cation and oxygen sites were refined using the SHELXL-14 software package [21], taking into account the atomic scattering curves for neutral atoms, with a semi-empirical (azimuthal scan) correction of absorption [22].

The $TlCdI_3$:Bi crystal was additionally studied on a Swiss-Norwegian Beamlines (SNBL) at the European Synchrotron Radiation Facility, Grenoble, France (SCXRD). The data were collected at 200(2) K (ω-scan mode). The wavelength of the synchrotron radiation was set to λ ~0.6999 Å. The data were recorded with single φ-scan and 0.1 slicing. The single-crystal data were preprocessed with SNBL Tool Box [23], the integral intensities were extracted from frames with CrysAlisPro software [24], and the crystal structure was refined with SHELXL-14 [21].

The structural parameters were refined in several steps. Initially, the positional and displacement parameters were simultaneously refined in isotropic and anisotropic approximations. Then the refinement of displacement parameters together with occupancy of Tl site was performed with fixed occupancies of Cd and Cl/I sites. Then the refinement of occupancy of Cd site was carried out with fixed occupancy of Cl/I site, and, finally, occupancy of Cl/I site was refined with fixed occupancy of Cd site. Due to the well-known correlation between displacement parameters and site occupancies we used the strategy of crystal structure refinement developed by us for both present objects and other complex oxides as described in detail [25,26]. After each refinement step, the residual electron density, displacement parameters, and interatomic distances were analyzed. The real compositions taking into account the electroneutrality, the correct values of the displacement parameters, the lowest values of the R factors, and the absence of residual electron-density peaks serve as criteria for the accuracy of the structure refinement and the correctness of the determination of the composition.

The EXAFS/XANES measurements of the $TlCdX_3$:Bi (X = Cl, I) (~100 mg) were performed at room temperature at the Structural Materials Science beamline of the Kurchatov synchrotron radiation source [27]. Samples

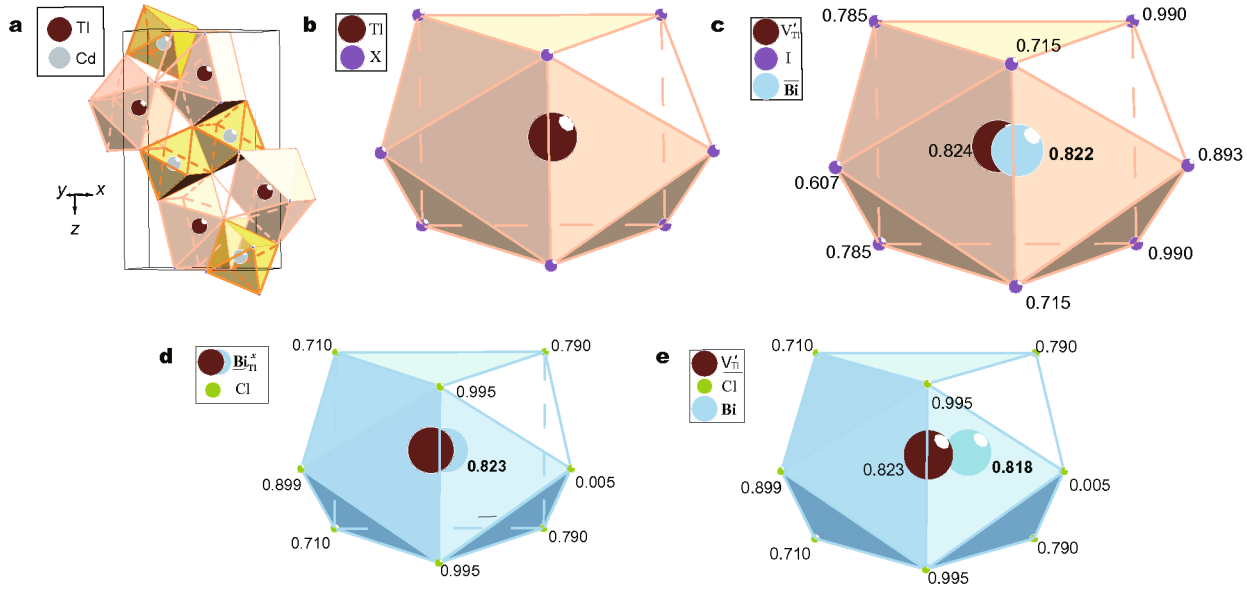

Figure 2 Structure of $TlCdX_3$ (X= Cl, I) (a), and TlX_8 (b), $(Tl,Bi_i)I_8$ (c), $(Tl,Bi)Cl_8$ (d), and $(Tl,Bi_i)Cl_8$ (e) coordination polyhedra.

were ground to a powder and evenly applied on the adhesive tape, having small X-ray absorption coefficient. The energy scans were performed using Si(220)-crystal monochromator with the energy resolution $\Delta E/E$ ~2×10^{-4}. The XAFS spectra were collected at the Tl and Cd K edges in a transmission mode, placing the sample between two ionization chambers connected to a picoammeter (Keithley), which also serves as a voltage source. The intensity of the monochromatic beam, incident on the sample and passing through it, was measured in air ionization chamber, filled with pure Ar up to atmospheric pressure, respectively.

The standard processing of experimental spectra was performed using an IFEFFIT program package [28]. The character of the atom's immediate environment was revealed by analyzing the radial distribution function $\varphi(r)$, obtained by Fourier transform of $k^3\cdot\chi(k)$ function during the experiment, where the multiplication by k^3 was used to compensate attenuation of Fourier transforms with distance from the absorption edge. Fourier transforms of EXAFS oscillations were extracted in the range of photoelectron wave number (k) from 2 to 12.0 $Å^{-1}$ at the both edges and modeled in the range of interatomic distance (d_{EXAFS}, Å) from 1.0 to 3.5 Å at the Tl edge, and from 1.0 to 3.2 Å at the Cd edge.

The photoluminescence spectra in the range of 880–1700 nm were obtained with a SDH-IV spectrometer (Solar LS), equipped with a G9212-512 InGaAs linear array photodetector (Hamamatsu). For photoluminescence excitation in the samples, compact laser modules, emitted at wavelengths of 405, 445, 450, 532, 635, 660, 685, 780, 808 and 820 nm, were used. The power of these sources was 20–400 mW. All the measurements were performed at room temperature.

The photoluminescence decay kinetics was studied at room temperature with a FLSP 920 fluorescence spectrophotometer (Edinburgh Instruments, UK) equipped with a xenon lamp.

RESULTS AND DISCUSSION

Structural studies

The $TlCdCl_3$ and $TlCdI_3$ compounds are isostructural and crystallize in the space group *Pnma* (Z = 4) (Fig. 2a). In the crystal structure, the Cd atoms are located in distorted octahedra with different interatomic distances (CN = 2 + 2 + 1 + 1; CN is coordination number), and the Tl atoms are in distorted bicapped trigonal prisms (CN = 2 + 2 + 2 + 1 + 1) (Fig. 2b).

The CdX_6 polyhedra as well as the TlX_8 ones are combined *via* edges to form chains along the ⟨110⟩ direction, whereas chains along the ⟨111⟩ direction are formed by alternation of the CdX_6 and TlX_8 polyhedra, connected also by edges (Fig. 2a).

Fig. 3 shows the correlation between the unit cell parameters of $TlCdX_3$ and the type of X atom [29,30]. A logical increase in the parameters with increasing radii of the X atoms ($R_I > R_{Br} > R_{Cl}$; R is an anion radius) is found.

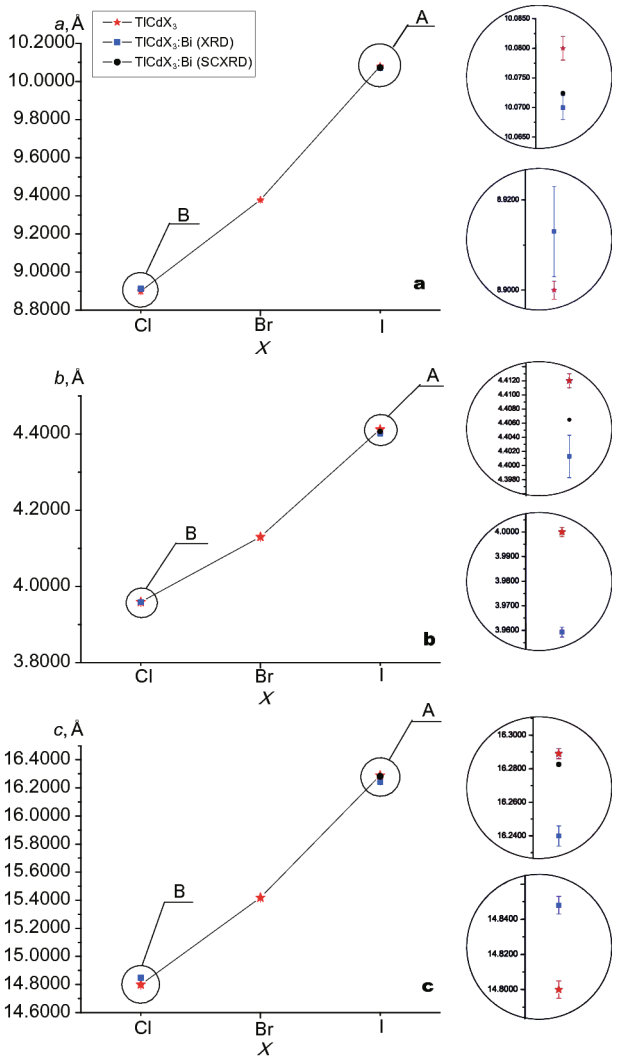

Figure 3 The relationship between the *a* (a), *b* (b), and *c* (c) unit cell parameters and type of the *X* anion in the $TlCdX_3$.

The unit cell parameters of $TlCdI_3$:Bi single crystals, determined by both XRD and SCXRD analyses (Table 1), are smaller than those found for the undoped $TlCdI_3$ crystals [30]. It follows that the Tl^+ ions (r_{Tl}^{VIII} = 1.59 Å [31]; *r* is a cation radius) are not replaced by the Bi^+ ones (r_{Bi}^{VIII} = 1.774 Å [12]), as was supposed [17,32–38]. The refinement of the Tl site occupancy showed its decrease, which also evidences an absence of the Bi^+ ions in this site (the form factor or atomic factor is proportional to the atomic number), but indicates the presence of vacancies (Table 1). The deficiency of the Tl site was found by both XRD and SCXRD analyses, but the defectiveness degree was different (Table 1), which may be explained by inhomogeneity of the crystal composition by volume. The deficiency of Cd and I site occupancies was not revealed.

The peak with $\Delta\rho_{max}$ = 3.08 was detected in the residual electron density of $TlCdI_3$:Bi sample. It can be responsible for the Bi^+ ions with a formal charge 1+ (according to the electroneutrality condition), located as interstitial atoms in the vicinity of the Tl^+ ions (Table 1, Fig. 2c). A defect formation in the $TlCdI_3$:Bi crystal can be described by a quasi-chemical reaction (Equation (1)):

$$0 \rightarrow V_{Tl}' + Bi_i^{\bullet}, \quad (1)$$

where V_{Tl}' is vacancy in Tl site ($'-$ negative-charged) and $Bi_i^{\bullet}$ is interstitial Bi atom ($^{\bullet}-$ positive-charged).

The unit cell parameters of undoped $TlCdCl_3$ crystals [29] are either smaller (the *a* and *c* parameters) or larger (the *b* parameter) than those found for the $TlCdCl_3$:Bi crystals (Fig. 3, Table 1). Therefore, the crystal structure of $TlCdCl_3$:Bi was refined under two assumptions (Models): the Bi^+ ions partially replace the Tl^+ ones (defined as Model 1, Fig. 2d) or Bi occupies interstitial sites (defined as Model 2, Fig. 2e). According to the Model 1, the refined composition was $(Tl_{0.78(15)}Bi_{0.22})CdCl_3$ (the final reliability factors were $S/R_1/wR_2$ = 1.137/0.0250/0.0550) without vacancies in the Cd and Cl sites; the quasi-chemical equation is

$$0 \rightarrow Bi_{Tl}^{\times}, \quad (2)$$

where $Bi_{Tl}^{\times}$ indicates a Bi atom replacing a Tl site ($^{\times}-$ neutral) (Fig. 2d). According to the Model 2, the refined composition was $Tl_{0.998(1)}Bi_{(i)0.005(1)}CdCl_3$ (the final reliability factors were $S/R_1/wR_2$ = 1.1220/0.0246/0.0546) with vacancies in the Tl site and interstitial Bi^+ ions; the quasi-chemical equation is as Equation (1) (Fig. 2e). As can be seen, the reliability factors are slightly better for the Model 2. Nevertheless, the simultaneous realization of both Models according to Equation (3)

$$0 \rightarrow V_{Tl}' + Bi_i^{\bullet} + Bi_{Tl}^{\times}, \quad (3)$$

as well as the formation of different associates containing the point defects observed, is possible for both $TlCdCl_3$:Bi and $TlCdI_3$:Bi crystals.

The greater content of interstitial Bi atoms in the vicinity of the Tl atoms in the $TlCdI_3$:Bi structure (Fig. 2c) compared with the $TlCdCl_3$:Bi one (Fig. 2e) is due to the larger radius of the I^- ions compared with Cl^- ones. The Tl–Bi*distance (Model 2) in the $TlCdCl_3$:Bi structure is greater than that in the $TlCdI_3$:Bi one (Tab. 1), which confirms the higher content of vacancies in the Tl site in the $TlCdI_3$:Bi structure. It should be noted that all the above-mentioned is concerned with the main point defects that can be detected by the XRD method with its sensitivity.

Table 1 Crystallographic data, experimental details and parameters, coordinates of atoms and their equivalent thermal parameters $U_{eq} \times 10^2$ (Å^2), site occupancies p (SOF), main interatomic distances d (Å), and refined compositions of $TlCdX_3$:Bi crystals according to the SXRD and XRD data

Chemical formula of the nominal composition	$TlCdI_3$:Bi		$TlCdCl_3$:Bi
Method	SXRD	XRD	
System, space group, Z		*Pnma*, $Z = 4$	
a (Å)	10.0724(2)	10.070(1)	8.913(2)
b (Å)	4.40649(6)	4.401(3)	3.959(2)
c (Å)	16.2826(3)	16.240(6)	14.848(5)
V (Å^3)	722.69	719.78	523.96
D_x (g cm^{-3})	6.410	6.436	5.364
Radiation λ (Å)	0.6999	Ag Kα; 0.5594	
Absorption μ (mm^{-1})	253.53	33.84	24.16
T (K)	200(2)	295(2)	
Sample size (mm)	> 0.1 × 0.1 × 0.1	~ 0.1 × 0.1 × 0.1	
Facility with the radiation source	Synchrotron SNBL beamline of ESRF	Enraf-Nonius CAD-4 diffractometer	
Type of scan	φ	ω	
$2\theta_{max}$ (°)	50.50	43.85	43.80
Limits h, k, l	$-11 \le h \le 11$, $-5 \le k \le 5$, $-18 \le l \le 18$	$-13 \le h \le 13$, $-5 \le k \le 5$, $-21 \le l \le 21$	$-11 \le h \le 11$, $-5 \le k \le 5$, $-19 \le l \le 19$
No. of reflections: measured/unique ($I > 2\sigma(I)$)	2598/664	1250/1011	777/740
No. of parameters in refinement	37		33
Weighting scheme	$1/[\sigma^2(F_0^2)+(0.0382P)^2+0.37P]$,	$1/[\sigma^2(F_0^2)+(0.0382P)^2+0.39P]$, $P = (F_0^2+2F_c^2)/3$	$1/[\sigma^2(F_0^2)+(0.0249P)^2+2.08P]$,
R_1 ($I > 2\sigma(I)$)	0.0385	0.0446	0.0250
wR_2	0.1069	0.1143	0.0554
S	1.113	1.247	1.137
Tl(*4c*)			
x	0.4371(4)	0.44212(2)	0.42999(4)
y	0.250	0.250	0.250
z	−0.17617(5)	−0.17563(2)	0.82319(2)
p	0.490(6)	0.3840(1)	0.39(7)
U_{eq}	0.0325(6)	0.03981(3)	0.0297(2)
Bi(*4c*)			
x	0.379(14)	0.41443(5)	0.5319(97)
yz	0.250 −0.177(3)	0.250 −0.17764(2)	0.250 0.818(4)
p	0.007(6)	0.1135(1)	0.0027(5)
U_{eq}	0.006(13)	0.03981(5)	0.0296(6)
Cd(*4c*)			
x	0.1676(1)	0.16764(2)	0.16849(7)
y	0.250	0.250	0.250
z	0.05630(7)	0.05631(2)	0.05615(4)
p	0.500	0.500	0.500
U_{eq}	0.0222(4)	0.02645(4)	0.0182(2)
$X1$(*4c*)			
x	0.1631(1)	0.16332(2)	0.2873(2)

(*To be continued on the next page*)

(*Continued*)

Chemical formula of the nominal composition	$TlCdI_3$:Bi		$TlCdCl_3$:Bi
y	0.250	0.250	0.250
z	0.48989(6)	0.48986(2)	0.2097(1)
p	0.500	0.500	0.500
U_{eq}	0.0190(4)	0.02134(3)	0.0234(4)
X2(4*c*)			
x	0.2915(1)	0.29108(2)	0.1680(2)
y	0.250	0.250	0.250
z	0.21462(6)	0.21401(2)	0.4954(1)
p	0.500	0.500	0.500
U_{eq}	0.0214(4)	0.02502(4)	0.0194(4)
X3(4*c*)			
x	0.0236(1)	0.02396(5)	0.0239(2)
y	0.250	0.250	0.250
z	−0.10712(6)	−0.10697(4)	0.8987(1)
p	0.500	0.500	0.500
pU_{eq}	0.0170(4)	0.01845(3)	0.0173(4)
Tl −2×*X*1	3.63110(15)	3.6322(2)	3.3492(2)
−1×*X*1	3.79230(15)	3.7501(2)	3.4294(2)
−2×*X*2	3.64950(15)	3.5283(2)	3.2416(2)
−2×*X*2	3.56620(15)	3.6836(2)	3.2413(2)
−1×*X*3	3.63460(15)	3.6255(3)	3.7890(2)
$[Tl–X]_{avr}$	3.64006	3.6330	3.3603
Cd−2×*X*1	2.9830(1)	2.9840(2)	2.6184(2)
−1×*X*2	2.8474(1)	2.8468(2)	2.5138(2)
−2×*X*3	3.0411(1)	3.0400(3)	2.7034(2)
−1×*X*3	3.0184(1)	3.0207(2)	2.6695(2)
Tl–Cd	4.2052	4.9032	4.5178
Tl–Bi[a]	0.5812	0.2486	0.9119
Refined compositions	$Tl_{0.980(12)}Bi_{(i)0.014(12)}CdI_3$	$Tl_{0.7680(6)}Bi_{(i)0.2270(6)}CdI_3$	$Tl_{0.78(15)}Bi_{0.22}CdCl_3$ (Model 1) $Tl_{0.998(1)}Bi_{(i)0.005(1)}CdCl_3$ (Model 2)

Note: The interatomic distance $d(Tl–Bi^{*})$ is the distance between centers of mass of Tl site ($Tl_{Tl}^{\times}$) or vacancies in this site (V_{Tl}') and atomic site with vacancies ($V_i^{\times}$) or interstitial Bi atoms ($Bi_i^{\bullet}$)

EXAFS/XANES spectroscopy

The XANES spectra measured at the Tl L_3-edge for $TlCdCl_3$:Bi and $TlCdI_3$:Bi samples (Fig. 4a, b) have pronounced differences in the intensity of the "white line" and some shifts of curves along the energy scale, but the general character of the spectra is similar for both samples. Such differences may be due to the fact that in the $TlCdCl_3$:Bi and $TlCdI_3$:Bi samples, having a similar local structures, the Tl ions are coordinated by the Cl and I ions, respectively.

The EXAFS Fourier transform curves measured at the Tl L_3-edge for the $TlCdCl_3$:Bi and $TlCdI_3$:Bi samples contain a series of peaks corresponding to the chlorine or iodine environment of Tl atoms (Fig. 4c). Table 2 contains the results of modelling the Tl environment using three nonequivalent paths of photoelectron scattering on Cl or I atoms. The modelling procedure results in the significantly reduced (d_{EXAFS} = 2.53 Å and 2.73 Å) and increased (d_{EXAFS} = 3.86 Å and 4.02 Å) values of several interatomic distances compared with the XRD data for the $TlCdCl_3$:Bi and $TlCdI_3$:Bi samples, respectively (Tables 1, 2). It may indicate the presence of vacancies either in the Cl (the coordination number have not been varied due to the large number of model parameters, but in sum, it should be one unit lower than the number of Cl atoms coordinated Bi atom according to the diffraction data) or Tl sites which is consistent with the XRD data (Table 1). The large values of the Debye parameters are due to the fact that the real nature of the coordination environment is more complicated than the indicated model.

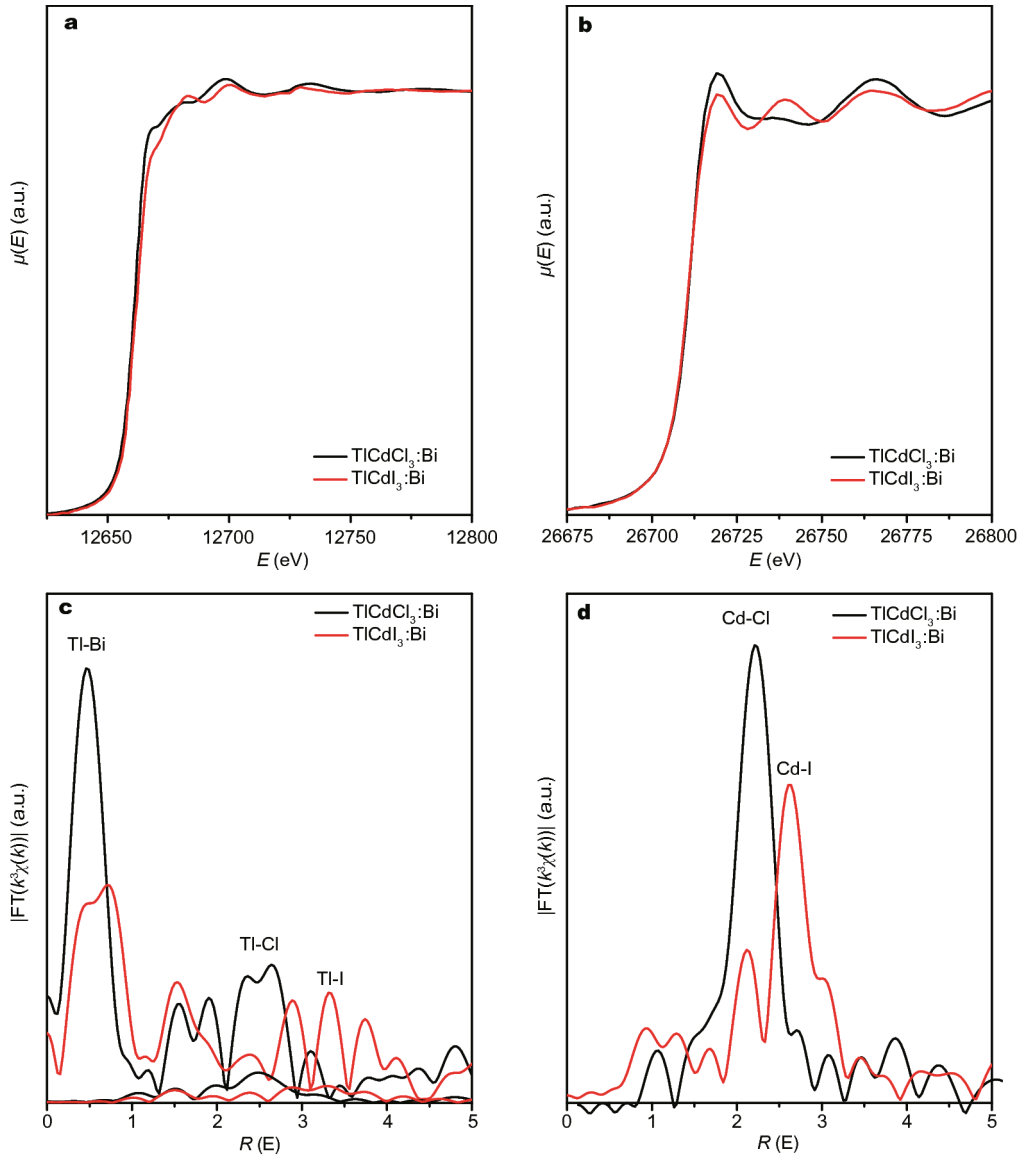

Figure 4 The XANES spectra (a, b) and EXAFS Fourier transform curves (c, d) measured at the Tl L_3-edge (a, c) and Cd K-edge (b, d) for $TlCdCl_3$:Bi and $TlCdI_3$:Bi crystals. A maximum noted as Ti-Bi can be either a physical maximum or an artifact of Fourier filtering.

Table 2 Structural parameters of the Tl local environment, obtained from the modeling of EXAFS Fourier transforms from the $TlCdCl_3$:Bi and $TlCdI_3$:Bi samples (σ^2, the Debye factor; CN, coordination number; R_f, the quadratic discrepancy)

Edge	Sample	Scattering path	d_{EXAFS} (Å)	σ^2 (Å^2)	CN	R_f (%)
Tl	$TlCdI_3$:Bi	Tl–I	3.86	0.0037	1.5	4.2
		Tl–I2	4.02	0.0011	0.7	
		Tl–I3	4.09	0.0154	3.0	
	$TlCdCl_3$:Bi	Tl–Cl1	2.53	0.0129	2.0	2.1
		Tl–Cl2	2.73	0.0100	2.0	
		Tl–Cl3	3.17	0.0191	2.0	
Cd	$TlCdCl_3$:Bi	Cd–Cl1	2.58	0.0026	1.3	2.6
		Cd–Cl2	2.71	0.0119	4.4	
	$TlCdI_3$:Bi	Cd–I1	2.87	0.0018	0.7	3.6
		Cd–I2	3.00	0.0107	3.8	

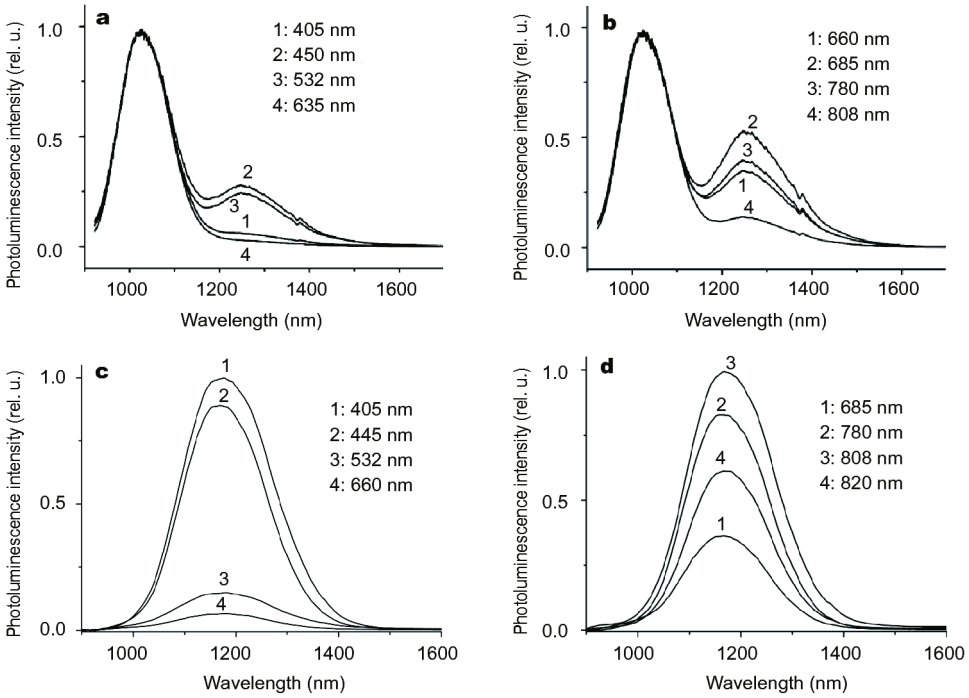

Figure 5 Photoluminescence spectra of $TlCdCl_3$:Bi (a, b) and $TlCdI_3$:Bi (c, d) samples recorded at room temperature with excitation with laser sources at different wavelengths.

The processing of EXAFS spectra usually includes a low-pass Fourier filtering, which excludes oscillations corresponding to the interatomic distances less than R_{bkg} ~1 Å. Such oscillations are either an artifact of the incorrect operation of monochromator or can be associated with the AXAFS-scattering of photoelectron emitted by atom on external electron shells of this atom or electron pairs formed covalent bonds. A decrease in the Fourier filtering level to R_{bkg} ~0.2 Å allows to reveal an intense peak at very small interatomic distances (~0.6 Å) (Fig. 4c, d). In our case, for predominantly ionic crystals, this peak can indicate the presence of Bi atoms at an ultra-short (1 Å and less) distance from Tl ones. The huge intensity of the peak is due to the fact that an atom located at a very small distance closes a large solid angle. The expected decrease in the peak intensity due to the relatively low occupancy of Bi interstitial site (in contrast to the AXAFS) is compensated by a high atomic number of the Bi atom, i.e., high electron density and atomic mass. Estimation of the interatomic distance and the coordination number of Tl–Bi* (Table 1) was not performed for this peak, since both intensity and peak location strongly depend on the Fourier filtering range.

The EXAFS Fourier transforms measured at the Cd K-edge for the $TlCdCl_3$:Bi and $TlCdI_3$:Bi samples have one significant peak, which is responsible for the chlorine or iodine environment of Cd atom (Fig. 4d). In the $TlCdCl_3$:Bi structure, there are four nonequivalent Cd–Cl distances. But it is reasonable not to consider such a large number of nonequivalent paths of photoelectron scattering since three of them are in the narrow range of 2.6–2.7 Å, taking into account an error in the determination of interatomic distances, which can exceed 0.05 Å for unequal but close distances. Hence, two independent scattering paths were considered. The CNs obtained are close to the volume value CN_{Cl} = 6, and the interatomic distances correspond to those found by the XRD analysis. High value of the Debye factor for a longer scattering path is due to the fact that this path corresponds to several nonequivalent scattering paths within the framework of the simplified model. These conclusions are related also to the $TlCdI_3$:Bi sample, wherein the Tl–I distances are greater than the Tl–Cl ones, hence, the shift of the most intense peak toward higher R values is observed in the curve measured for the $TlCdI_3$:Bi (Fig. 4d). A weak peak at R ~2.2 Å, coinciding in position with the Cd–Cl peak, is not associated with the presence of chloride. It can be explained by interference phenomena during the photoelectron scattering on nonequivalent I atoms.

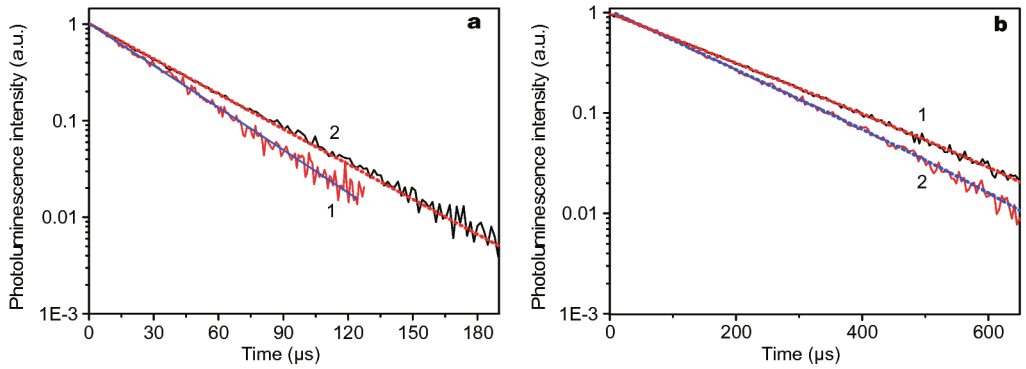

Figure 6 Decay curves of photoluminescence peaked at 1035 (1) and 1270 nm (2) under excitation at 620 and 690 nm for the $TlCdCl_3$:Bi sample (a) and decay curves of photoluminescence peaked at 1170 nm under excitation at 740 (1) and 350 nm (2) for the $TlCdI_3$:Bi (b). The approximation of the obtained curves by a single-exponential function is shown.

Optical properties

The photoluminescence spectra of $TlCdCl_3$:Bi and $TlCdI_3$:Bi single-crystal samples excited with light with different wavelengths are given in Fig. 5. Comparison of the spectra of both samples indicates their obvious differences, which is consistent with the XRD and EXAFS/XANES results. The differences are related to the number of photoluminescence bands (there are two bands for $TlCdCl_3$:Bi, and one band for $TlCdI_3$:Bi) and to the shift of the band with λ ~1200 nm to ~1253 and ~1175 nm for the $TlCdCl_3$:Bi and $TlCdI_3$:Bi, respectively (Fig. 5) [38,39].

The position of the first photoluminescence band with λ ~1025 nm in the spectra of $TlCdCl_3$:Bi sample (Fig. 5) corresponds to the emission of the Bi^+ cation [19]. The nature of the second optically active center (photoluminescence band with a maximum at λ ~1253 nm) was unclear. According to the results of present work, the band with λ ~1025 nm can really be due to the presence of Bi^+ ions at the Tl^+ site, and the second band with λ ~1253 nm is associated with interstitial Bi^+ atoms (Equation (3)). This conclusion is confirmed by the results of XRD study of $TlCdI_3$:Bi crystals: in all the spectra of the $TlCdI_3$:Bi sample, the photoluminescence band with λ ~1000 nm is absent (Fig. 5), and only one broad intense photoluminescence band with a maximum at λ ~1175 nm occurs, which is probably due to a high concentration of interstitial Bi atoms (Equation (1)) caused by a shift in the luminescence band (Fig. 5). It should be noted that these discussions and conclusions are related to main point defects, which, in turn, can enter into associates of different types and compositions.

Despite the similarity of the spectra of $TlCdI_3$:Bi given in Fig. 5c, d, they are slightly different in the intensities at the center and at the wings of the band. It indicates that there is one photoluminescent center in the sample responsible for most of the emitted radiation. However, along with it, the sample under investigation contains one or more radiating centers, which contribute insignificantly to the overall photoluminescence signal. The emission of these centers causes differences in the photoluminescence spectra obtained with the excitation at different wavelengths.

The photoluminescence decay from the $TlCdI_3$:Bi and $TlCdCl_3$:Bi samples after photoexcitation with a pulsed light source was studied (Fig. 6).

Fig. 6 shows that the photoluminescence decay from both samples is well described by a one-exponential model. The characteristic lifetimes are 30 μs (1) and 35 μs (2) for the $TlCdI_3$:Bi (Fig. 6b). Due to the fact that the Bi^+-doped $RbAlCl_4$, $CsAlCl_4$, $RbMgCl_3$, $CsMgCl_3$, $KCdCl_3$ and $RbCdCl_3$ crystals were found to possess the long-lived luminescence from 280 μs to 525 μs [19], the Bi^+ ion can hardly be the source of photoluminescence from the $TlCdI_3$:Bi sample. The characteristic lifetimes are 150 μs (1) and 170 μs (2) for the $TlCdCl_3$:Bi (Fig. 6a). It is assumed that the appearance of IR photoluminescence bands in the $TlCdCl_3$:Bi is apparently due to the optical transitions between the energy levels of the Bi^+ cation located in a crystalline environment (field), similar to the $KMgCl_3$:Bi crystals, which also possess long-lived luminescence [17].

CONCLUSIONS

The Bi^+-doped $TlCdCl_3$ and $TlCdI_3$ single crystals have been investigated by XRD analysis using X-ray and synchrotron radiation with the subsequent refinement of site occupancies and analysis of the residual electron density as well as EXAFS/XANES spectroscopy. In addition, the

photoluminescent properties have been studied for both samples.

The crystals studied here have precise real compositions $Tl_{0.7680(6)}Bi_{(i)0.2270(6)}CdI_3$ and $Tl_{0.998(1)}Bi_{(i)0.005(1)}CdCl_3$ with vacancies in the Tl sites (V_{Tl}') and interstitial Bi atoms ($Bi_i^{\bullet}$) and defect-free Cd ($Cd_{Cd}^{\times}$) and I or Cl ($X_X^{\times}$) sites. The presence of Bi ions in the Tl site, i.e., $(Tl,Bi)_{0.998(1)}Bi_{(i)0.005(1)}CdCl_3$, is possible for the $TlCdCl_3$:Bi^{1+} sample.

The $TlCdCl_3$:Bi^{1+} single crystals are characterized by two optical centers (λ ~1025 nm and λ ~1253 nm), which corresponds to the presence of Bi^+ ions in the Tl^+ sites ($Bi_{Tl}^{\times}$) and interstitial Bi atoms ($Bi_i^{\bullet}$), respectively. Interstitial Bi atoms ($Bi_i^{\bullet}$) are responsible for one optical center (λ ~1175 nm) in $TlCdI_3$:Bi single crystal. Associates comprising of these point defects and vacancies in the Tl site (V_{Tl}') may also affect an appearance of the optical centers.

The wide luminescence band, non-hygroscopicity and easiness of obtaining Bi^+-doped $TlCdCl_3$ and $TlCdI_3$ single-crystals make them attractive for potential applications in photonics.

Received 20 July 2017; accepted 12 September 2017; published online 13 October 2017

1 Peng M, Da N, Krolikowski S, *et al.* Luminescence from Bi_{2+}-activated alkali earth borophosphates for white LEDs. Opt Express, 2009, 17: 21169–21178
2 Ahmed E, Köhler D, Ruck M. Room-temperature synthesis of bismuth clusters in ionic liquids and crystal growth of $Bi_5(AlCl_4)_3$. Z anorg allg Chem, 2009, 635: 297–300
3 Cao R, Peng M, Wondraczek L, *et al.* Superbroad near-to-mid-infrared luminescence from Bi_5^{3+} in $Bi_5(AlCl_4)_3$. Opt Express, 2012, 20: 2562–2571
4 Wosylus A, Dubenskyy V, Schwarz U, *et al.* Dynamic disorder of Bi_8^{2+} clusters in the plastic phase $(Bi\text{-}_8)_3Bi[InI_4]_9$. Z anorg allg Chem, 2009, 635: 1030–1035
5 Kuznetsov AN, Naumenko PI, Popovkin BA, *et al.* New representative of Bi_9^{5+} -containing phases: synthesis and crystal structure of the Nb^{IV}-containing $Bi_{10}Nb_3Cl_{18}$ compound. Rus Chem Bull, 2003, 52: 2100–2104
6 Dai D, Whangbo MH, Ugrinov A, *et al.* Analysis of the effect of spin–orbit coupling on the electronic structure and excitation spectrum of the Bi_2^{2-} anion in $(K\text{-crypt})_2Bi_2$ on the basis of relativistic electronic structure calculations. J Phys Chem A, 2005, 109: 1675–1683
7 Sun H T, Zhou J, Qiu J. Recent advances in bismuth activated photonic materials. Prog Mater Sci, 2014, 64: 1–72
8 Davis HL, Bjerrum NJ, Smith GP. Ligand field theory of p2,4 configurations and its application to the spectrum of Bi^+ in molten salt media. Inorg Chem, 1967, 6: 1172–1178
9 Meng XG, Qiu JR, Peng MY, *et al.* Near infrared broadband emission of bismuth-doped aluminophosphate glass. Opt Express, 2005, 13: 1628–1634
10 Bjerrum NJ, Boston CR, Smith GP. Lower oxidation states of bismuth. Bi+ and $[Bi_5]^{3+}$ in molten salt solutions. Inorg Chem, 1967, 6: 1162–1172
11 Kuznetsov AN, Popovkin BA, Henderson W, *et al.* Monocations of bismuth and indium in arene media: a spectroscopic and EXAFS investigation. J Chem Soc Dalton Trans, 2000, 2000: 1777–1781
12 Romanov AN, Grigoriev FV, Sulimov VB. Estimation of Bi^+ monocation crystal ionic radius by quantum chemical simulation. Comp Theor Chem, 2013, 1017: 159–161
13 Ruan J, Su L, Qiu J, *et al.* Bi-doped BaF_2 crystal for broadband near-infrared light source. Opt Express, 2009, 17: 5163–5169
14 Su L, Zhao H, Li H, *et al.* Near-infrared ultrabroadband luminescence spectra properties of subvalent bismuth in CsI halide crystals. Opt Lett, 2011, 36: 4551–4553
15 Su L, Zhao H, Li H, *et al.* Near-infrared photoluminescence spectra in Bi-doped CsI crystal: evidence for Bi-valence conversions and Bi ion aggregation. Opt Mater Express, 2012, 2: 757–764
16 Li C, Song Z, Qiu J, *et al.* Broadband yellow–white and near infrared luminescence from Bi-doped $Ba_{10}(PO_4)_6Cl_2$ prepared in reductive atmosphere. J Lumin, 2012, 132: 1807–1811
17 Romanov AN, Veber AA, Fattakhova ZT, *et al.* Subvalent bismuth monocation Bi^+ photoluminescence in ternary halide crystals $KAlCl_4$ and $KMgCl_3$. J Lumin, 2013, 134: 180–183
18 Romanov A N, Fattakhova Z T, Veber A A, *et al.* On the origin of near-IR luminescence in Bi-doped materials (II) Subvalent monocation Bi^+ and cluster Bi_5^{3+} luminescence in $AlCl_3/ZnCl_2/BiCl_3$ chloride glass. Opt Express, 2012, 20: 7212
19 Vtyurina D N, Romanov A N, Veber A A, *et al.* The spectral properties and the NIR photoluminescence of univalent bismuth Bi + in $RbAlCl_4$, $CsAlCl_4$, $RbMgCl_3$, $CsMgCl_3$, $KCdCl_3$ and $RbCdCl_3$ crystal phases. Russ J Phys Chem B, 2016, 10: 388–393
20 Farrugia LJ. *WinGX* suite for small-molecule single-crystal crystallography. J Appl Crystlogr, 1999, 32: 837–838
21 Gruene T, Hahn H W, Luebben A V, *et al.* Refinement of macromolecular structures against neutron data with *SHELXL2013*. J Appl Crystlogr, 2014, 47: 462–466
22 North ACT, Phillips DC, Mathews FS. A semi-empirical method of absorption correction. Acta Cryst A, 1968, 24: 351–359
23 Dyadkin V, Pattison P, Dmitriev V, *et al.* A new multipurpose diffractometer PILATUS@SNBL. J Synchrotron Rad, 2016, 23: 825–829
24 CrysAlisPro Software system, Version 1.171.37.35, Agilent Technologies, Oxford, 2014
25 Kaurova IA, Kuz'micheva GM, Rybakov VB, *et al.* Composition, structural parameters, and color of langatate. Inorg Mater, 2010, 46: 988–993
26 Kuz'micheva GM. Some Aspects of the Applied Crystallochemistry. Moscow: MIREA, 2016 [in Russian]
27 Trofimova NN, Veligzhanin AA, Murzin VY, *et al.* Structural diagnostics of functional nanomaterials with the use of X-ray synchrotron radiation. Nanotechnol Russia, 2013, 8: 396–401
28 Ravel B, Newville M. *ATHENA*,*ARTEMIS*,*HEPHAESTUS*: data analysis for X-ray absorption spectroscopy using *IFEFFIT*. J Synchrotron Rad, 2005, 12: 537–541
29 Bogdanova AV, Zaslavskaya NP, Sinichka EV, et al. Synthesis and crystal structure of $TlCdCl_3$ and $TlCdBr_3$. Inorg Mater, 1993, 29: 664–666
30 Zandbergen HW, Verschoor GC, IJdo DJW. The structures of thallium cadmium triiodide and dirubidium iron tetraiodide. Acta Crystlogr B Struct Sci, 1979, 35: 1425–1427
31 Shannon RD. Revised effective ionic radii and systematic studies of interatomic distances in halides and chalcogenides. Acta Cryst A,

1976, 32: 751–767
32 Veber AA, Romanov AN, Usovich OV, *et al.* Luminescent properties of Bi-doped polycrystalline $KAlCl_4$. Appl Phys B, 2012, 108: 733–736
33 Romanov A N, Veber A A, Fattakhova Z T, *et al.* Spectral properties and NIR photoluminescence of Bi^+ impurity in $CsCdCl_3$ ternary chloride. J Lumin, 2014, 149: 292–296
34 Veber AA, Romanov AN, Usovich OV, *et al.* Optical properties of the Bi^+ center in $KAlCl_4$. J Lumin, 2014, 151: 247–255
35 Romanov AN, Veber AA, Vtyurina DN, *et al.* NIR photoluminescence of bismuth-doped $CsCdBr_3$—the first ternary bromide phase with a univalent bismuth impurity center. J Lumin, 2015, 167: 371–375
36 Romanov AN, Veber AA, Vtyurina DN, *et al.* Near infrared photoluminescence of the univalent bismuth impurity center in leucite and pollucite crystal hosts. J Mater Chem C, 2015, 3: 3592–3598
37 Okhrimchuk AG, Butvina LN, Dianov EM, *et al.* Near-infrared luminescence of $RbPb_2Cl_5$:Bi crystals. Opt Lett, 2008, 33: 2182–2184
38 Vtyurina DN, Romanov AN, Kuznetsov MS, *et al.* Optical properties of bismuth-doped $TlCdCl_3$ crystal. Russ J Phys Chem B, 2016, 10: 1–4
39 Romanov AN, Vtyurina DN, Haula EV, *et al.* Broadband infrared photoluminescence of $TlCdI_3$ iodide doped with bismuth. Russ J Phys Chem B, 2017, 11: 83–86

Acknowledgements The authors express sincere gratitude to SNBL beamline of ESRF for its hospitality.

Author contributions Vtyurina DN designed and engineered the samples as well as performed optical investigations; Eistrikh-Geller PA performed the structural data analysis; Kuz'micheva GM wrote the paper with support from Kaurova IA; Rybakov VB performed the X-ray diffraction analysis; Khramov EV performed the EXAFS/XANES measurements; Chernyshov DY performed the experiment using synchrotron radiation, Korchak VN performed optical investigations. All authors contributed to the general discussion.

Conflict of interest The authors declare that they have no conflict of interest.

Daria Vtyurina received her bachelor degree (2006) and master degree (2009) from the Lomonosov Moscow State University and PhD (2017) from Semenov Institute of Chemical Physics, Russian Academy of Science. From 2008 to 2011, she works as a senior researcher at the Lomonosov Moscow State University. She joined Semenov Institute of Chemical Physics as a senior researcher in 2012. Her research interests include the spectroscopy and the photoluminescence in crystals.

Irina Kaurova received her bachelor degree (2005), master degree (2007), and PhD (2010) from the Moscow State Academy of Fine Chemical Technology. From 2010 to 2014, she works as an associate professor at the Moscow State Open University. She joined Moscow Technological University as senior researcher in 2014. Her research interests include the solid state chemistry and characterization of functional materials.